We are IntechOpen, the world's leading publisher of Open Access books Built by scientists, for scientists

4,800
Open access books available

122,000
International authors and editors

135M
Downloads

Our authors are among the

154
Countries delivered to

TOP 1%
most cited scientists

12.2%
Contributors from top 500 universities

CLARIVATE ANALYTICS BOOK CITATION INDEX INDEXED

WEB OF SCIENCE™

Selection of our books indexed in the Book Citation Index in Web of Science™ Core Collection (BKCI)

Interested in publishing with us?
Contact book.department@intechopen.com

Numbers displayed above are based on latest data collected.
For more information visit www.intechopen.com

13

A Novel Frequency Tracking Method Based on Complex Adaptive Linear Neural Network State Vector in Power Systems

M. Joorabian, I. Sadinejad and M. Baghdadi
Shahid Chamran University
Iran

1. Introduction

In some digital application systems, power system frequency tracking is an important task. Accurate power frequency estimation is a necessity to check the state of health of power index, and a guarantee for accurate quantitative measurement of power parameters such as voltages, currents, active power and reactive power, in multi-function power meters under steady states. Many researches have been done in this area.
Three criteria that a frequency tracking method should satisfy is given as follows (Akke,1997):

1. Fast speed of convergence
2. Accuracy of frequency estimation
3. Robustness to noise.

He compares traditional modulation with new modulation. Traditional demodulation introduces a double frequency component that needs to be filtered away. For signals with low noise, the filter to reduce the double frequency component can often limit the speed of the frequency estimation algorithm. The purpose of this section is to show that the proposed method eliminates this problem. If other filters are the bottle-neck of the estimation algorithm, we will not capitalise on the benefits.
Many well-proven techniques such as zero-crossing technique, level-crossing technique, least squares error technique, Newton method, Kalman filter, Fourier transform, and wavelet transform have been used for power harmonic frequency estimation in the fields of measurement, instrumentation, control and monitoring of power systems. Besides, a comprehensive analysis of discrete Fourier transform (DFT) error is given in some researches, including the cases of synchronous sampling and error rises when sampling frequency does not synchronize with signal frequency. A frequency tracking method based on linear estimation of phase (LEP) has been introduced. Also, a processing unit for symmetrical components and harmonic estimation based on an adaptive linear combiner has been proposed.
This section presents the application of a complex adaptive linear neural network (CADALINE) in tracking the fundamental power system frequency. In this method, by using stationary-axes Park transformation in addition to producing a complex input measurement, the decaying DC offset is effectively eliminated. As the proposed method uses a first-order differentiator to estimate frequency changes, a Hamming filter is used to

smoothen the response and cancel high-frequency noises. The most distinguishing features of the proposed method are the reduction in the size of observation state vector required by a simple adaptive linear neural network (ADALINE) and increase in the accuracy and convergence speed under transient conditions. This section concludes with the presentation of the representative results obtained in numerical simulations and simulation in PSCAD/EMTDC software as well as in practical study.

2. ADALINE structure to track fundamental frequency

Figure 1 depicts the ADALINE structure to track fundamental frequency which is a proposed in this section.

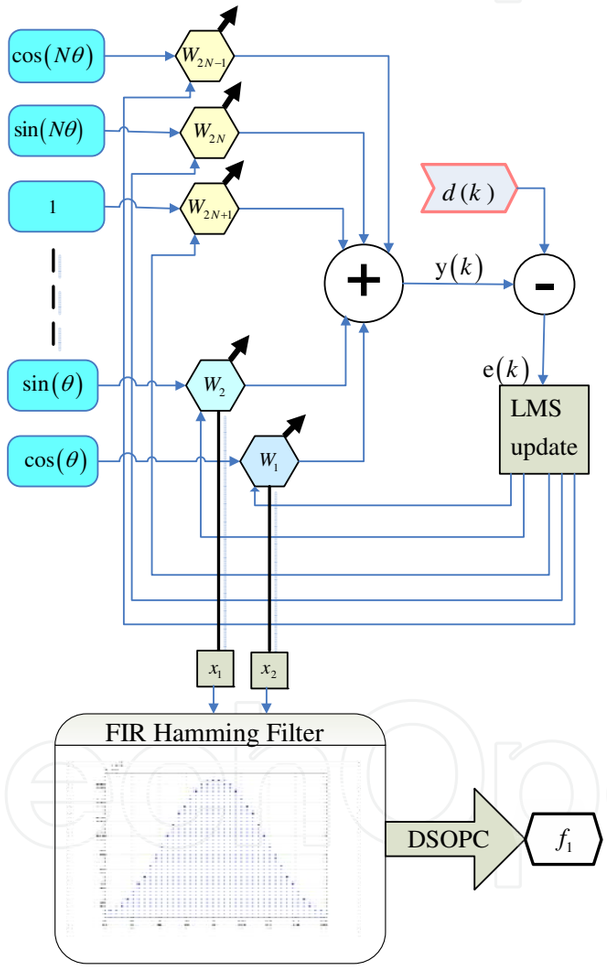

Fig. 1. ADALINE structure to track fundamental frequency

Assume that the voltage waveform of power system comprises unknown fundamental, harmonics and decaying DC offset components as:

$$V(t) = \sum_{l=1}^{N} V_l \sin\left(l\omega_0 t + \Phi_1\right) + A_v e^{\left(-\frac{t}{\tau}\right)} \tag{1}$$

where V_1 and Φ_1 are the amplitude and phase of the fundamental frequency respectively. A_v and τ are the amplitude and time constant of decaying DC offset respectively; N is the total number of harmonics; and ω_0 is the fundamental angular frequency in (rad/sec). Time-discrete expression of (1) is:

$$V(k)=\sum_{l=1}^{N} V_l \sin(l\theta+\Phi_1)+A_v e^{\left(-\frac{\theta}{\tau.\omega_0}\right)} \tag{2}$$

where $\theta = 2\pi k / N_s$ and N_s is sampling rate given by $N_s = \frac{f_s}{f_0}$, in which f_s is sampling frequency and f_0 is fundamental frequency of power system. By using the triangular equality:

$$\sin(\alpha+\beta)=\sin(\alpha)\cos(\beta)+\sin(\beta)\cos(\alpha) \tag{3}$$

Equation (2) can be rewritten as:

$$V(k)=\sum_{l=1}^{N} V_l \sin(\Phi_l)\cos(l\theta)+V_l\cos(\Phi_l)\sin(l\theta)+A_v e^{\left(-\frac{\theta}{\tau.\omega_0}\right)} \tag{4}$$

Rearranging the above equation in the matrix form, we obtain:

$$V(k)=\Psi_V \times X^T(k) \tag{5}$$

where $V(k)$ represents the measurement at each sampling, $X(k)$ is the time varying observation matrix and Ψ_V is the parameter at each iteration to be tracked. $X(k)$ and Ψ_V are shown in the following formula:

$$\begin{aligned}\Psi_V &= \begin{bmatrix} V_1\sin(\Phi_1) & V_1\cos(\Phi_1) & V_2\sin(\Phi_2) & V_2\cos(\Phi_2) \\ \dots & V_N\sin(\Phi_N) & V_N\cos(\Phi_N) & A_v \quad -\frac{A_v}{\tau} \end{bmatrix} \\ X(k) &= \begin{bmatrix} \cos(\theta) & \sin(\theta) & \cos(2\theta) & \sin(2\theta) \\ \dots\cos(N\theta) & \sin(N\theta) & 1 & -\frac{\theta}{\omega_0} \end{bmatrix}\end{aligned} \tag{6}$$

According to Fig. 1, at kth iteration, the input vector $X(k)$ is multiplied by the weighting vector $W(k)=\left[w_1(k)w_2(k)\dots w_P(k)\right]$, and then these weighted inputs are summed to produce the linear output $y(k)=W(k)\times X(k)^T$. In order for the ADALINE output to precisely mimic the desired value $d(k)$, the weight vector is adjusted utilizing an adaptation rule that is mainly based on least mean square (LMS) algorithm. This rule is also known as Widrow–Hoff delta rule [27] and is given by:

$$W(k+1)=W(k)+\frac{\alpha\, e(k)X(k)}{X(k)\times X(k)^T} \tag{7}$$

where α is the constant learning parameter and $e(k)=y(k)-d(k)$ is the error. When perfect learning is attained, the error is reduced to zero and the desired output becomes equal to $d(k)=W_0\times X(k)^T$, where W_0 is the weight vector after the complete algorithm convergence. Thus, the neural model exactly predicts the incoming signal. To track harmonic components of a voltage signal with ADALINE, the variables $\Psi_V(k)$ and $V(k)$ are simply assigned to $W(k)$ and $d(k)$ respectively, with $P=2\times N+2$.
After mentioned error converges to zero, the weight vector yields the Fourier coefficients of power signal as:

$$W_0=\begin{bmatrix} V_1\sin(\Phi_1) & V_1\cos(\Phi_1) & V_2\sin(\Phi_2) & V_2\cos(\Phi_2) \\ \dots & V_N\sin(\Phi_N) & V_N\cos(\Phi_N) & A_v \quad -\dfrac{A_v}{\tau} \end{bmatrix} \tag{8}$$

Voltage amplitude and phase angle of N^{th} harmonic are:

$$\begin{aligned} V_N &= \sqrt{W_0^2(2N-1)+W_0^2(2N)} \\ \Phi_{V,N} &= \tan^{-1}\left(W_0(2N-1)\Big/W_0(2N)\right) \end{aligned} \tag{9}$$

Voltage amplitude and phase angle of fundamental frequency extracted by (9) are:

$$\begin{aligned} V_1 &= \sqrt{W_0^2(1)+W_0^2(2)} \\ \Phi_{V,1} &= \tan^{-1}\left(W_0(1)\Big/W_0(2)\right) \end{aligned} \tag{10}$$

By sampling current signal with the same approach, discrete expression of current is:

$$I(k)=\sum_{l=1}^{N} I_l\sin(\Phi_l)\cos(l\theta)+I_l\cos(\Phi_l)\sin(l\theta)+A_i e^{\left(-\frac{\theta}{\omega_0.\tau}\right)} \tag{11}$$

in which, variables $\Psi_I(k)$ and $I(k)$ are simply assigned to $W(k)$ and $d(k)$ respectively, with $P=2\times N+2$ [27]. $\Psi_I(k)$ is defined as:

$$\Psi_I=\begin{bmatrix} I_1\sin(\Phi_1) & I_1\cos(\Phi_1) & I_2\sin(\Phi_2) & I_2\cos(\Phi_2) \\ \dots & I_N\sin(\Phi_N) & I_N\cos(\Phi_N) & A_i \quad -\dfrac{A_i}{\tau} \end{bmatrix} \tag{12}$$

Current amplitude and phase of N^{th} harmonic are calculated as follows:

$$\begin{aligned} I_N &= \sqrt{W_0^2(2N-1)+W_0^2(2N)} \\ \Phi_{I,N} &= \tan^{-1}\left(W_0(2N-1)\Big/W_0(2N)\right) \end{aligned} \tag{13}$$

Current amplitude and phase of fundamental frequency are achieved by:

$$I_1 = \sqrt{W_0^2(1) + W_0^2(2)}$$
$$\Phi_{I,1} = \tan^{-1}\left(W_0(1) \Big/ W_0(2)\right) \tag{14}$$

To track frequency, a center frequency is assumed to be the actual value. It would be the operational frequency of the power system which is usually 50 Hz or 60 Hz. Under situations that the base power frequency changes, the k^{th} sample of fundamental component of voltage or current signal is modeled:

$$s(kT_s) = A \cdot \sin(2\pi f_x kT_s + \phi) \tag{15}$$

that can be rewritten as:

$$s(kT_s) = x_1 \sin(2\pi \cdot f_0 \cdot k \cdot T_s) + x_2 \cos(2\pi \cdot f_0 \cdot k \cdot T_s) \tag{16}$$

Where x_1 is the in-phase component, x_2 is the quadrature phase component, f_0 is the center frequency (60 Hz), f_1 is the frequency deviation, and T_s is the sampling interval $\left(\frac{1}{f_s}\right)$. Before calculating the frequency deviation (f_1), x_1 and x_2 pass through a FIR Hamming window and parameters y_1 and y_2 are obtained as:

$$y_1(kT_s) = \sum_{i=1}^{N_0} x_1\left((k-i+1)\cdot T_s\right) \times H(i)$$
$$y_2(kT_s) = \sum_{i=1}^{N_0} x_2\left((k-i+1)\cdot T_s\right) \times H(i) \tag{17}$$

where $H(i)$ is the i^{th} coefficient of the FIR Hamming window coefficients and N_0 is the sampling rate given by $N_0 = \left(\frac{f_s}{f_0}\right)$. The cut frequency for the low pass Hamming window is 20 Hz and the length of filter is 40. Fig. 2 shows the impulse response of this Hamming window. By using DSOPC principle, f_1 is obtained as:

$$f_1(kT_s) = \frac{1}{2\pi} \times \frac{y_1(kT_s)y_2'(kT_s) - y_2(kT_s)y_1'(kT_s)}{(y^2{}_2(kT_s) + y^2{}_1(kT_s))} \tag{18}$$

y_1' and y_2' are first-order discrete derivatives defined as:

$$y_1'(kT_s) = \frac{y_1(kT_s) - y_1(kT_s - T_s)}{T_s}$$
$$y_2'(kT_s) = \frac{y_2(kT_s) - y_2(kT_s - T_s)}{T_s} \tag{19}$$

Finally, the real value of fundamental frequency (f_x) is calculated by adding the frequency deviation to the assumed center frequency as:

$$f_x = f_0 + f_1 \tag{20}$$

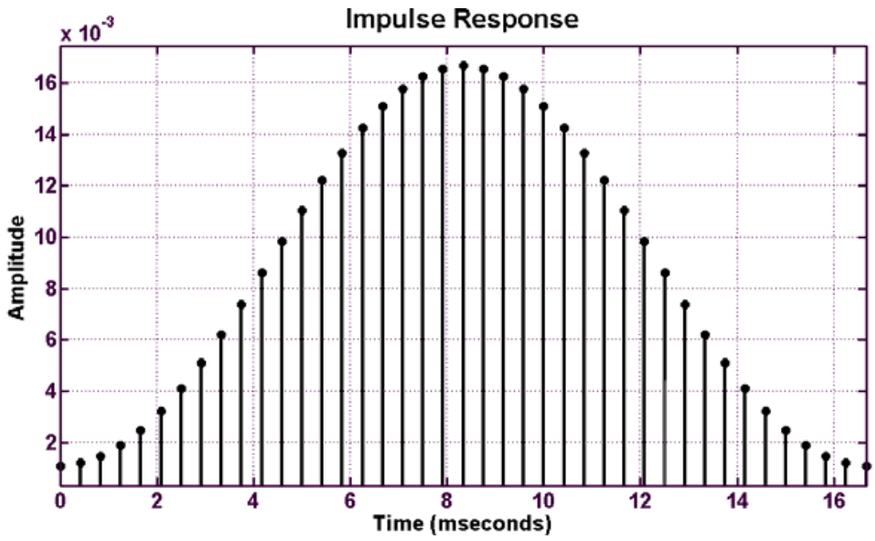

Fig. 2. Impulse response of the Hamming window with 20 Hz cut frequency

3. Complex ADALINE structure to track fundamental frequency

The proposed complex ADALINE (CADALINE) structure is based on the Widrow–Hoff delta rule, explained earlier. The improvement in ADALINE structure is made by introducing a complex observation vector. This approach reduces the number of weight updates, and so, the number of parameters to be estimated. To produce a complex vector measurement the use of the stationary-axes Park transformation is proposed. Stationary-axes Park transformation is widely employed to study the behavior of rotating electrical machines in transient conditions. However, it can be considered a more general and powerful tool to study the behavior of three-phase systems. This transformation applied to the signals $y_a(t), y_b(t)$ and $y_c(t)$ (voltages or currents) of a three-phase system leads to the Park components $y_d(t)$, $y_q(t)$ and $y_0(t)$ defined as:

$$\begin{bmatrix} y_d \\ y_q \\ y_0 \end{bmatrix} = [T] . \begin{bmatrix} y_a \\ y_b \\ y_c \end{bmatrix} \tag{21}$$

where $[T]$ is the orthogonal matrix defined as:

$$T = \begin{bmatrix} \sqrt{\frac{2}{3}} & -\sqrt{\frac{1}{6}} & -\sqrt{\frac{1}{6}} \\ 0 & \sqrt{\frac{1}{2}} & -\sqrt{\frac{1}{2}} \\ \sqrt{\frac{1}{3}} & \sqrt{\frac{1}{3}} & \sqrt{\frac{1}{3}} \end{bmatrix} \tag{22}$$

In the *d-q* frame, it is then possible to define the Park vector as a complex quantity as:

$$y = y_d + jy_q \tag{23}$$

This vector is used as a desired value. The complex observation matrix Z is introduced by:

$$Z(kT_s) = \left[e^{j\omega_0 kT_s},\quad e^{j2\omega_0 kT_s},\quad \ldots\quad e^{jN\omega_0 kT_s},\quad 1,\quad -kT_s \right]^T \tag{24}$$

ω_0 is the center angular frequency (rad/sec), defined as $\omega_0 = 2\pi f_0$. The complex harmonic vector to be tracked at k^{th} sample is $\Gamma(kT_s)$ and is defined as:

$$\Gamma(kT_s) = \left[A_1(kT_s),\quad A_2(kT_s)\quad \ldots\quad A_N(kT_s),\quad A_{N+1}(kT_s),\quad A_{N+2}(kT_s) \right]^T \tag{25}$$

where $A_1(kT_s)$ is the complex phasorial expression of center frequency in the *d-q* frame. According to LMS rule, weight update is:

$$\Gamma(kT_s) = \Gamma(kT_s - T_s) + \alpha \cdot \vec{e}(kT_s - T_s) \frac{Z(kT_s - T_s)}{Z^T(kT_s - T_s) \cdot Z(kT_s - T_s)} \tag{26}$$

$\vec{e}(kT_s)$ is the complex error obtained as follows:

$$\begin{aligned} Y_s(kT_s) &= \Gamma^T(kT_s) \times Z(kT_s) \\ \vec{e}(kT_s) &= Y_s(kT_s) - y(kT_s) \end{aligned} \tag{27}$$

where $Y_s(kT_s)$ is the complex estimation of the actual values of $y(kT_s)$ in *d-q* frame.

It should be noted that under conditions where power system operates with the nominal frequency, $A_1(kT_s)$ is a constant vector, which does not rotate with respect to the time in the complex frame. When the base frequency changes, $A_1(kT_s)$ becomes a rotating vector. It is the result of the fact that when the base frequency changes, $A_1(kT_s)$ components appear as modulated signals and their carrier is the occurred frequency-drift. Therefore, the rate of this rotation is the key element to track the frequency deviation from the center frequency. The frequency deviation (f_1) is achieved by normalizing and differentiating $A_1(kT_s)$. For the types of power swing events studied here, it has been found that the non-fundamental components cannot be characterized as harmonics. A middle-filter is, therefore, required so that the signal is dominated by the fundamental component. The middle-filter, used here, is the FIR Hamming type filter as has been used in [18]. It is the same which has been used in Section 2. $A_1(kT_s)$ passes through the FIR Hamming window and $Ah_1(kT_s)$ is obtained as:

$$Ah_1(kT_s) = \sum_{i=1}^{N_0} \left[A_1\left((i-k+1)T_s\right) \cdot H(i) \right] \tag{28}$$

$Ah_1(kT_s)$ should be normalized to produce the rotating operator ($e^{(j2\pi f_1 kT_s)}$). $e^{(j2\pi f_1 kT_s)}$ stands for a normal rotating vector which its amplitude is unity and f_1 is the frequency deviation. Therefore, complex normalized rotating state vector $An_1(kT_s)$ is obtained as:

$$An_1(kT_s) = \frac{Ah_1(kT_s)}{abs\left(Ah_1(kT_s)\right)} \tag{29}$$

where $abs(x)$ stands for absolute value of x. By using the first-order discrete differentiator, f_1 is obtained as:

$$f_1(kT_s) = \left(\frac{1}{j2\pi \cdot An_1 \cdot k \cdot T_s}\right) \cdot \left(\frac{An_1(kT_s) - An_1(kT_s - T_s)}{T_s}\right) \tag{30}$$

It can be seen that observation matrix size and the parameters to be estimated have been reduced to $(N+2)$ elements in comparison with the simple ADALINE which uses $(2N+2)$ elements. Furthermore, owing to the fact that data from three phases are combined, the most important aspect of the proposed technique is that the convergence speed is considerably improved. After all, decaying DC offset is effectively eliminated by applying stationary-axes Park transformation and using CADALINE. Fig. 3 shows the complex ADALINE structure to track fundamental frequency.

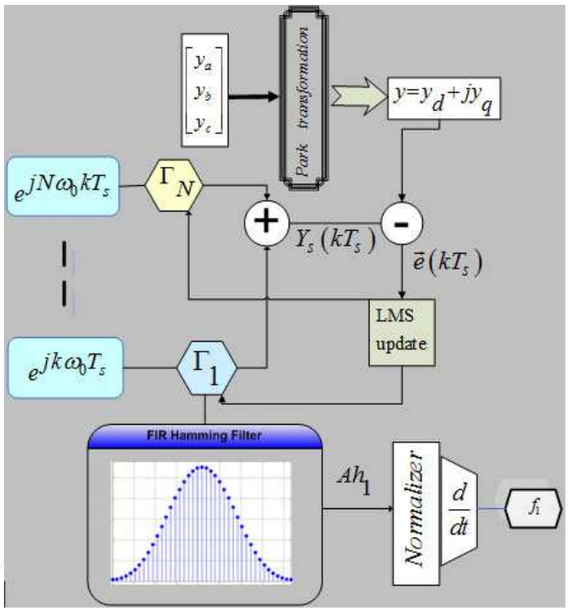

Fig. 3. Complex ADALINE structure to track fundamental frequency

4. Review of Kalman and DFT approaches

4.1 Kalman filter to track fundamental frequency

Kalman filter has also been used to track fundamental frequency in power system. Consider the following deterministic state-variable equation for a periodic signal having harmonic components up to N^{th} order with samples z_k, at time t_k, $(2n+1)$ samples per period.

$$\begin{aligned} x_{k+1} &= F \times x_k \\ z_k &= Q \times x_k \end{aligned} \tag{31}$$

where $(2N+1)$-dimensional state vector x_k is as follows:
$x_k(2i-1)$: real component of the i^{th} harmonic phasor,
$x_k(2i)$: imaginary component of the i^{th} harmonic phasor,
$x_k(2i+1)$: decaying DC component,
where the i^{th} element of x_k is represented by $x_k(i)$, and F is:

$$F=\begin{bmatrix} f(1\psi) & 0 & \cdots & 0 & 0 \\ 0 & f(2\psi) & \cdots & 0 & 0 \\ \vdots & \vdots & \cdots & \vdots & \vdots \\ 0 & 0 & \cdots & f(N\cdot\psi) & \vdots \\ 0 & 0 & \cdots & 0 & 1 \end{bmatrix} \tag{32}$$

where $\psi=\omega_0 T_s$, ω_0 is the fundamental supply angular frequency in (rad/sec) and T_s is the sampling interval in seconds.

$$f(i\psi)=\begin{bmatrix} \cos(i\psi) & -\sin(i\psi) \\ \sin(i\psi) & \cos(i\psi) \end{bmatrix} \quad i=1,2,\ldots,N \tag{33}$$

and Q is a ($1 \times (2n+1)$) matrix which gives the connection between the measurement (z_k) and the state vector (x_k). The sampled value of the signal is considered to be the sum of the real components of the harmonic phasors and the decaying DC component. Therefore, Q is given by:

$$Q=[1,0,1,0,\cdots,1,0,1] \tag{34}$$

The harmonic components h_i (RMS) are given by:

$$h_i^2=\frac{\left(x_k^2(2i-1)+x_k^2(2i)\right)}{2} \quad i=1,2,\ldots,N \tag{35}$$

The problem of estimating the present state of the signal model (Eq. 31) from measurements (z_k) involves the design of standard state observers [33]. The observer state can be represented by:

$$\hat{x}_{k+1}=F\times\hat{x}_k+P\times(z_k-Q\hat{x}_k) \tag{36}$$

where $\hat{x}_k$ denotes the estimate of the state vector x_k and P is the observer gain matrix. The primary objective in choosing P is to obtain a stable observer, which is achieved by assigning the eigenvalues of the matrix $F-PQ$ within the unit circle. The locations of the eigenvalues determine, among other things, the transient response of the observer. For the purpose of frequency tracking, the speed of response and tracking ability are of particular importance. After studying various choices, the following case is considered.

$$\begin{aligned} P=[&0.248,0.0513,0.173,0.046,0.0674,0.0434,0.00916,\\ &0.0236,-0.000415,0.113,0.0802]^T \end{aligned} \tag{37}$$

To estimate fundamental frequency, the approach is based on DSPOC which has been described in Eqs. 15–20 is used.

4.2 DFT filter to track fundamental frequency

Under situation of frequency change, the k^{th} sample of fundamental voltage or current signal is described as denoted in Eq. 15. By using a DFT dynamic window, parameters x_1 and x_2 in Eq. 16 can be achieved as follows:

$$x_1(kT_s) = (\frac{2}{N_s}) \sum_{k=0}^{N_s-1} \left[s(kT_s) \cdot sin(2\pi \frac{k}{N_s}) \right]$$
$$x_2(kT_s) = (\frac{2}{N_s}) \sum_{k=0}^{N_s-1} \left[s(kT_s) \cdot cos(2\pi \frac{k}{N_s}) \right] \quad (38)$$

The fundamental frequency tracking process includes the same approach that has been expressed in Eqs. 15–20.

5. Adaptive linear element

ADALINE (Adaptive Linear Neuron or later Adaptive Linear Element) is a single layer neural network as the 'least mean square' (LMS) learning procedure, also known as the delta

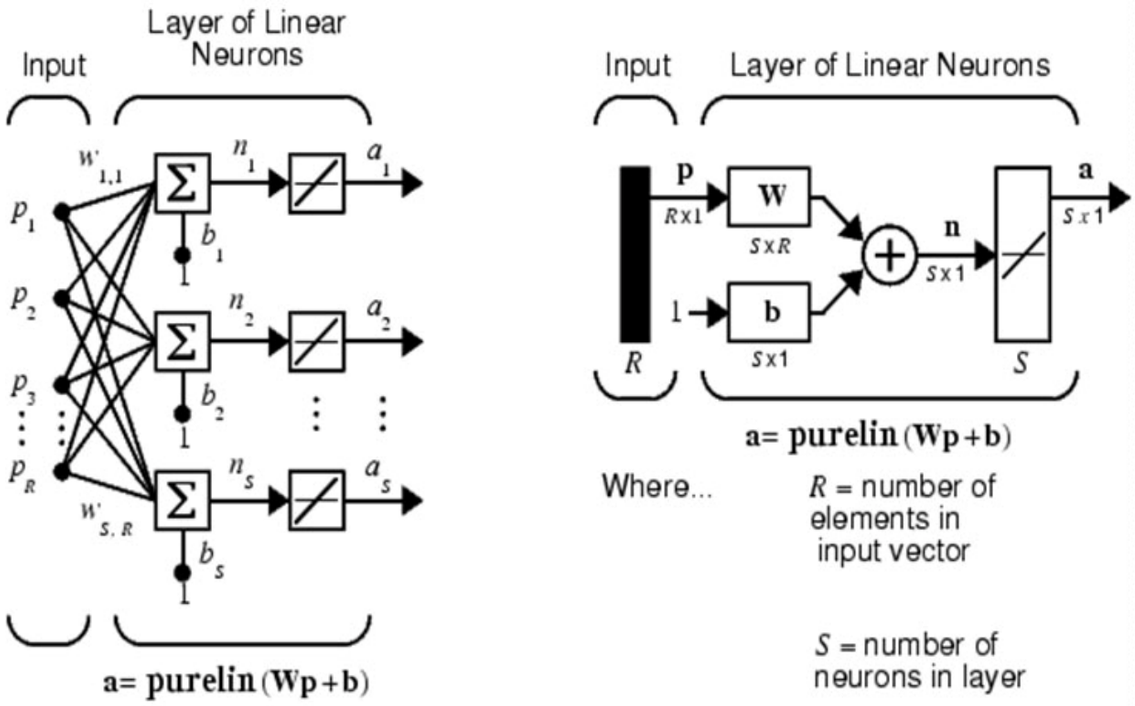

rule. It was developed by ProfessorBernard Widrow and his graduate student Ted Hoff at Stanford University in 1960. It is based on the McCulloch–Pitts neuron. It consists of a weight, a bias and a summation function.The difference between Adaline and the standard (McCulloch-Pitts) perceptron is that in the learning phase the weights are adjusted according to the weighted sum of the inputs (the net). In the standard perceptron, the net is passed to the activation (transfer) function and the function's output is used for adjusting the weights. The main functional difference with the perceptron training rule is the way the output of the system is used in the learning rule. The perceptron learning rule uses the output of the threshold function (either -1 or +1) for learning. The delta-rule uses the net output without further mapping into output values -1 or +1. The ADALINE network shown below has one layer of S neurons connected to R inputs through a matrix of weights W.
This network is sometimes called a MADALINE for Many ADALINEs. Note that the figure on the right defines an *S*-length output vector a.
The Widrow-Hoff rule can only train single-layer linear networks. This is not much of a disadvantage, however, as single-layer linear networks are just as capable as multilayer linear networks. For every multilayer linear network, there is an equivalent single-layer linear network.

5.1 Single ADALINE

Consider a single ADALINE with two inputs. The following figure shows the diagram for this network.

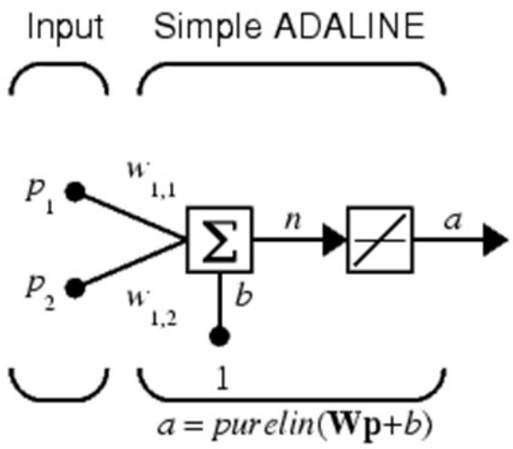

The weight matrix W in this case has only one row. The network output is:

$$a = purelin(n) = purelin(Wp + b) = (Wp + b) \tag{39}$$

Equation a can be written as follows:

$$a = w_{1,1}p_1 + w_{1,2}p_2 + b \tag{40}$$

Like the perceptron, the ADALINE has a decision boundary that is determined by the input vectors for which the net input n is zero. For n = 0 the equation Wp + b = 0 specifies such a decision boundary, as shown below:

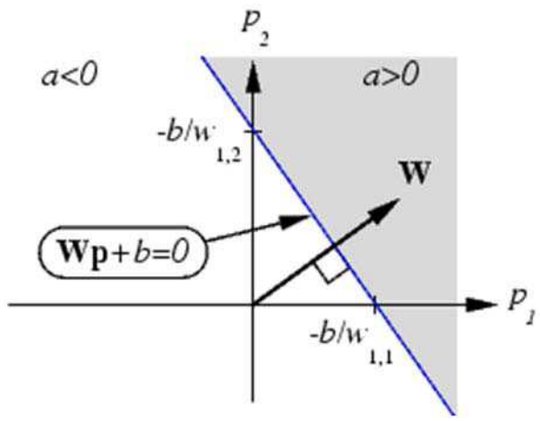

Input vectors in the upper right gray area lead to an output greater than 0. Input vectors in the lower left white area lead to an output less than 0. Thus, the ADALINE can be used to classify objects into two categories.
However, ADALINE can classify objects in this way only when the objects are linearly separable. Thus, ADALINE has the same limitation as the perceptron.

5.2 Networks with linear activation functions: the delta rule

For a single layer network with an output unit with a linear activation function the output is simply given by:

$$y = \sum_{i=1}^{n} w_i x_i + \theta \tag{41}$$

Such a simple network is able to represent a linear relationship between the value of the output unit and the value of the input units. By thresholding the output value, a classifier can be constructed (such as Widrow's Adaline), but here we focus on the linear relationship and use the network for a function approximation task. In high dimensional input spaces the network represents a (hyper) plane and it will be clear that also multiple output units may be defined. Suppose we want to train the network such that a hyper plane is fitted as well as possible to a set of training samples consisting of input values d_p and desired (or target) output values d_p. For every given input sample, the output of the network differs from the target value d_p by $\left(d^p - y^p\right)$ where y_p is the actual output for this pattern. The delta-rule now uses a cost- or error-function based on these differences to adjust the weights. The error function, as indicated by the name least mean square, is the summed squared error. That is, the total error E is denoted to be:

$$E = \sum_p E^p = \frac{1}{2}\sum_p \left(d^p - y^p\right)^2 \tag{42}$$

Where the index p ranges over the set of input patterns and E_p represents the error on pattern p. The LMS procedure finds the values of all the weights that minimize the error function by a method called gradient descent. The idea is to make a change in the weight proportional to the negative of the derivative of the error as measured on the current pattern with respect to each weight:

$$\Delta_p w_j = -\gamma \frac{\partial E^p}{\partial w_j} \tag{43}$$

where γ is a constant of proportionality. The derivative is

$$\frac{\partial E^p}{\partial w_j} = \frac{\partial E^p}{\partial y^p}\frac{\partial y^p}{\partial w_j} \tag{44}$$

$$\frac{\partial y^p}{\partial w_j} = x_i \tag{45}$$

Because of the linearity, $\frac{\partial E^p}{\partial w_j}$ is as follows:

$$\frac{\partial E^p}{\partial w_j} = -\left(d^p - E^p\right) \tag{46}$$

Where $\delta^p = d^p - E^p$ is the difference between the target output and the actual output for pattern p .The delta rule modifies weight appropriately for target and actual outputs of either polarity and for both continuous and binary input and output units. These characteristics have opened up a wealth of new applications.

6. Simulation results

Simulation examples include the following three categories. Numerical simulations are represented in Section 5.1. for two cases, simulation in PSCAD/EMTDC software is presented in Section 5.2. Lastly, Section 5.3. presents practical measurement of a real fault incidence in Fars province, Iran.

6.1 Simulated signals

Herein, a disturbance is simulated at time 0.3 sec. Three-phase non-sinusoidal unbalanced signals, including decaying DC offset and third harmonic, are produced as:

$$\begin{cases} V_A = 220\sin(\omega_0 t) \\ V_B = 220\sin(\omega_0 t - \frac{2\pi}{3}) \\ V_C = 220\sin(\omega_0 t + \frac{2\pi}{3}) \end{cases} \quad 0 \le t \le 0.3 \tag{47}$$

After disturbance at 0.3 sec, signals are:

$$\begin{cases} V_A = 400\sin(\omega_x t) + 40\sin(3\omega_x t) + 400e^{(-10t)} \\ V_B = 800\sin(\omega_x t - \frac{2\pi}{3}) + 60\sin(3\omega_x t) + 800e^{(-10t)} \\ V_C = 800\sin(\omega_x t + \frac{2\pi}{3}) + 20\sin(3\omega_x t) \end{cases} \quad 0.3 \le t \le 0.6 \tag{48}$$

where ω_0 is the base angular frequency and ω_x is the actual angular frequency after disturbance.

6.1.1 Case 1

In this case, a 1-Hz frequency deviation occurs and tracked frequency using CADALINE, ADALINE, Kalman, and DFT approaches is revealed in Fig. 4; three-phase signals are shown in Fig. 5. Estimation error percentage according to the samples fed to each algorithm after frequency drift is shown in Fig. 6. Second set of samples including 100 samples, equivalent to two and half cycles, which is fed to all algorithms is magnified in Fig. 6. It can be seen that CADALINE converges to the real value after first 116 samples, less than three power cycles, with error of -0.4 %; and reaches a perfect estimation after having more few samples. Other methods' estimations are too fare from real value in this snapshoot. DFT, ADALINE and Kalman respectively need 120, 200 and 360 samples to reach less than one percent error in estimating the frequency drift. It should be considered that for 2.4-kHz sampling frequency and power system frequency of 60 Hz, each power cycle includes 40 samples. The complex normalized rotating state vector $An_1(kT_s)$ with respect to time and in *d-q* frame is shown in Fig. 7. It has been seen that for 1-Hz frequency deviation ($f_1 = 1$ Hz), CADALINE has the best convergence response in terms of speed and over/under shoot. ADALINE method convergence speed is half that in the CADALINE and shows a really high overshoot. Besides, Kalman approach shows the biggest error. in the first 7 power system cycles, it converges to 61.7 Hz instead of 61 Hz and its computational burden is considerably higher than other methods. In this case, presence of a long-lasting decaying DC offset affects the DFT performance. Consequently, its convergence speed and overshoot are not as improved as CADALINE.

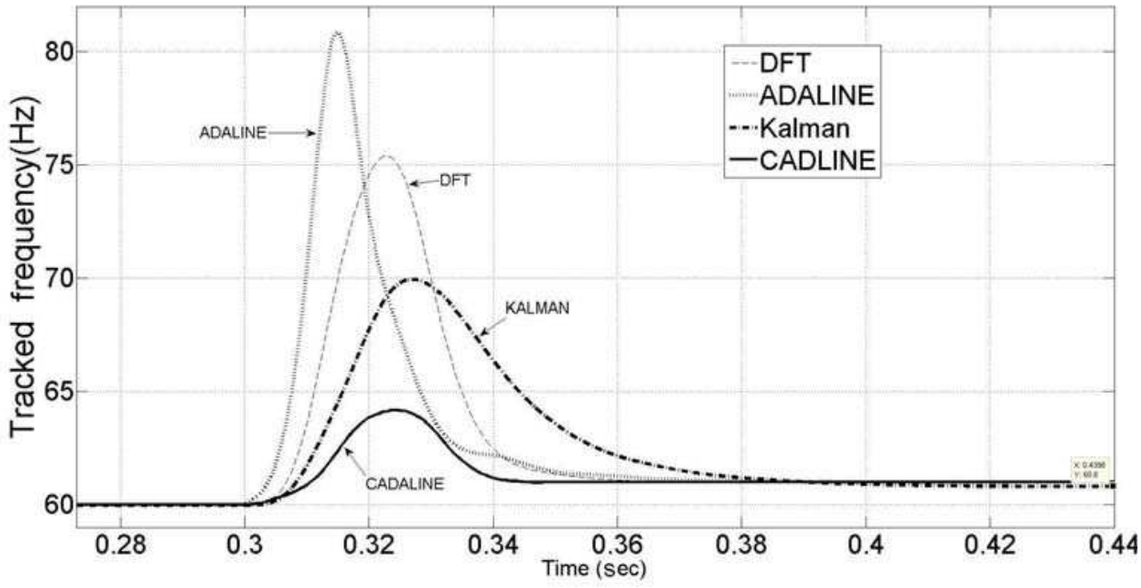

Fig. 4. Tracked frequency (Hz)

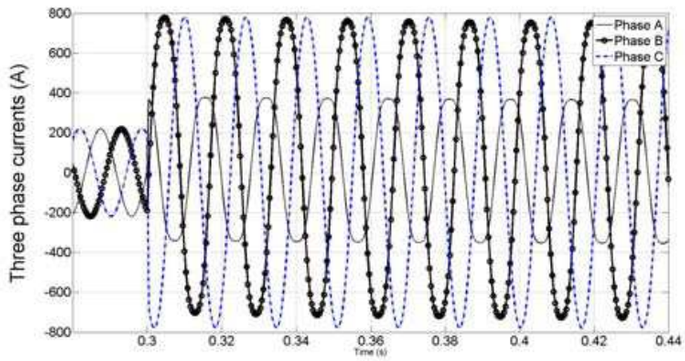

Fig. 5. Three-phase signals

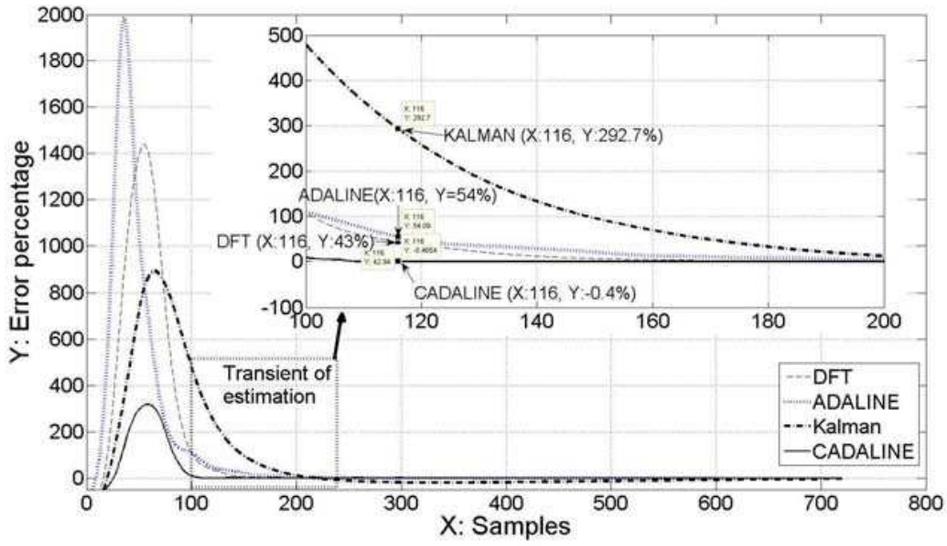

Fig. 6. Estimation error percentage according to samples fed to each algorithm after frequency drift

As can be seen in Fig. 7, $An_1(kT_s)$ starts rotation simultaneously when the frequency changes at time 0.3 sec.

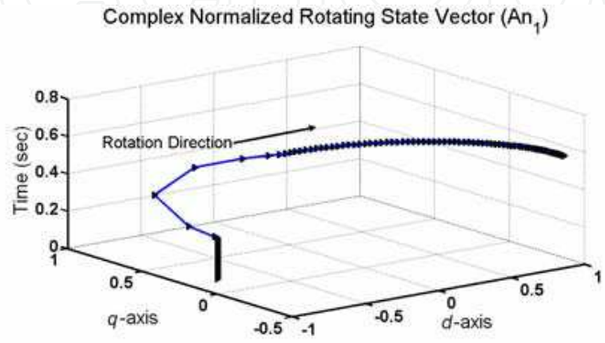

Fig. 7. Complex normalized rotating state vector (An_1)

6.1.2 Case 2

In this case, a three-phase balanced voltage is simulated numerically. The only change applied is a step-by-step 1-Hz change in fundamental frequency to study the steady-state response of the proposed method when the power system operates under/over frequency conditions. The three-phase signals are:

$$\begin{cases} V_A = 220\sin(\omega_x t) \\ V_B = 220\sin(\omega_x t - \frac{2\pi}{3}) \\ V_C = 220\sin(\omega_x t + \frac{2\pi}{3}) \end{cases} \quad (49)$$

where $\omega_x = 2\pi f_x$, and values of f_x are shown in Table I. The range of frequency that has been studied here is 50–70 Hz. Results are revealed in Table I and average convergence time is shown in Fig. 8 for CADALINE, ADALINE, Kalman filter and DFT approaches. The results from this section can give an insight into the number of samples that each algorithm needs to converge to a reasonable estimation. According to the fact that each power cycle is equivalent to 40 samples, average number of samples that is needed for each algorithm to have estimation with less than one percent error is represented in Table I.

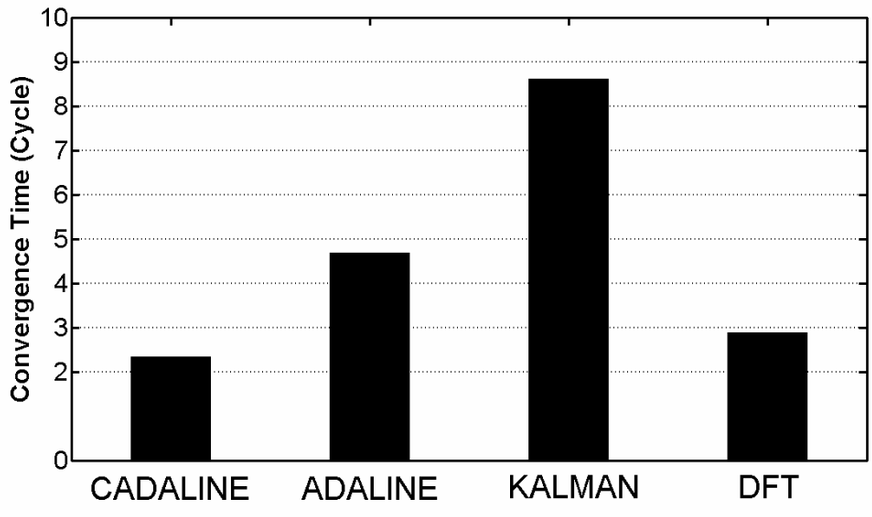

Fig. 8. Average convergence time (cycles) to track static frequency changes

6.2 Simulation in PSCAD/EMTDC software

In this case, a three-machine system controlled by governors is simulated in PSCAD/EMTDC software, shown in Fig. 9. Information of the simulated system is given in Appendix I. A three-phase fault occurs at 1 sec. Real frequency changes, estimation by use of ADALINE, CADALINE and Kalman approaches are shown in Fig. 10. Instead of DFT method, the frequency measurement module (FMM) performance which exists in PSCAD library is compared with the presented methods. Phase-A voltage signal is shown in Fig. 11.

	Approaches			
f_x(Hz)	**CADALINE**	**KALMAN**	**ADALINE**	**DFT**
70	95	360	202	111
69	97	421	188	114
68	93	358	186	118
67	90	384	187	114
66	95	385	178	114
65	97	305	138	139
64	92	361	211	114
63	93	328	193	116
62	98	430	206	115
61	96	360	231	116
60	92	385	220	112
59	83	234	155	97
58	81	281	181	116
57	88	313	197	117
56	98	216	178	123
55	97	377	192	117
54	96	336	206	122
53	90	331	195	114
52	96	290	190	108
51	96	374	184	120
50	105	405	113	112

Table I Samples needed to estimate with 1 percent error for 50-70 frequency range

The complex normalized rotating state vector ($An_1(kT_s)$) is shown in Fig. 12. The best transient response and accuracy belongs to ADALINE and CADALINE, but CADALINE has faster response with a considerable lower overshoot, as can be seen in Fig. 10. Kalman

approach has a suitable response in this case, but its error and overshoot in estimating frequency are bigger than that in CADALINE. The PSCAD FMM shows drastic fluctuations in comparison with other methods proposed and reviewed here.

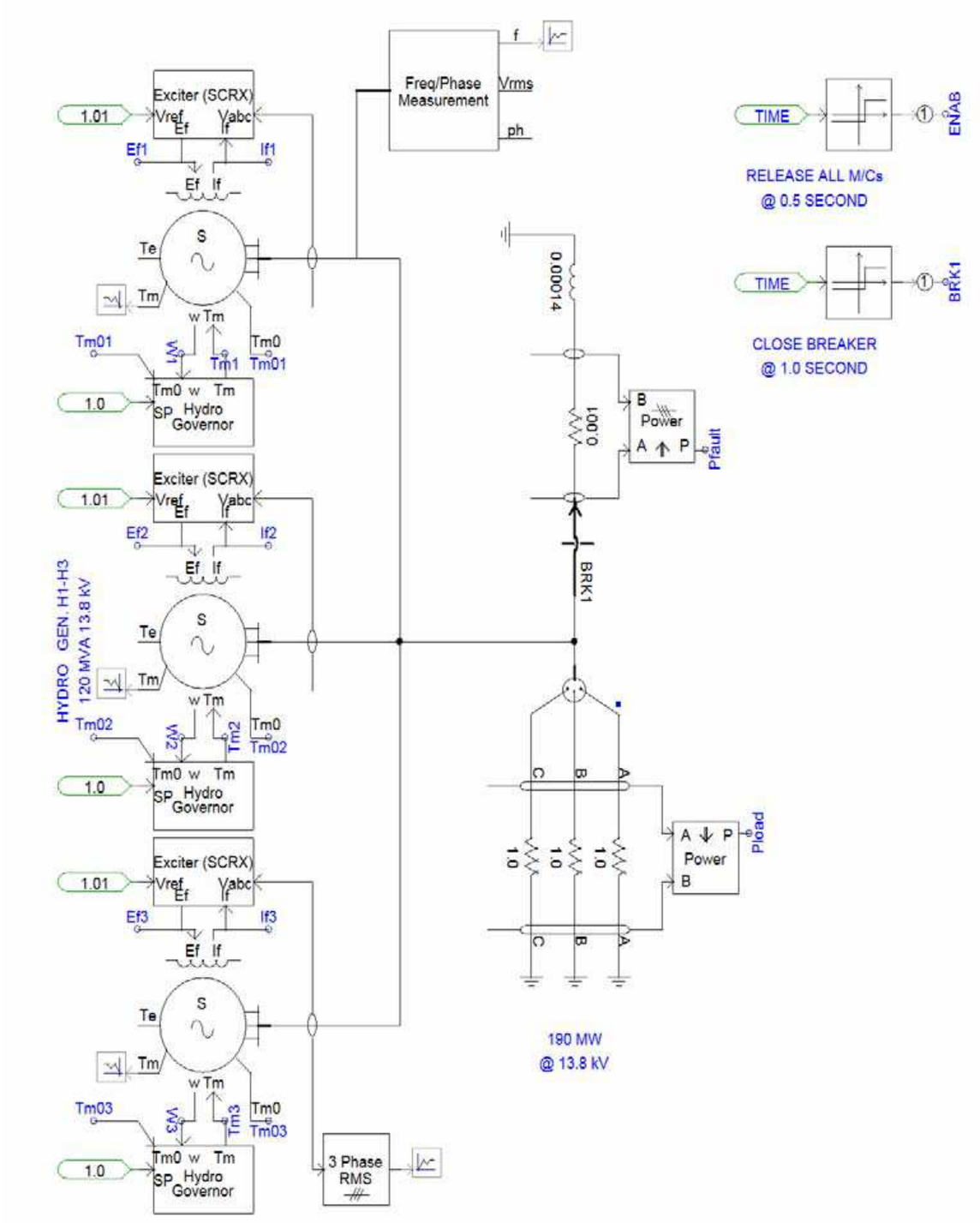

Fig. 9. A three-machine connected system simulated in PSCAD/EMTDC software

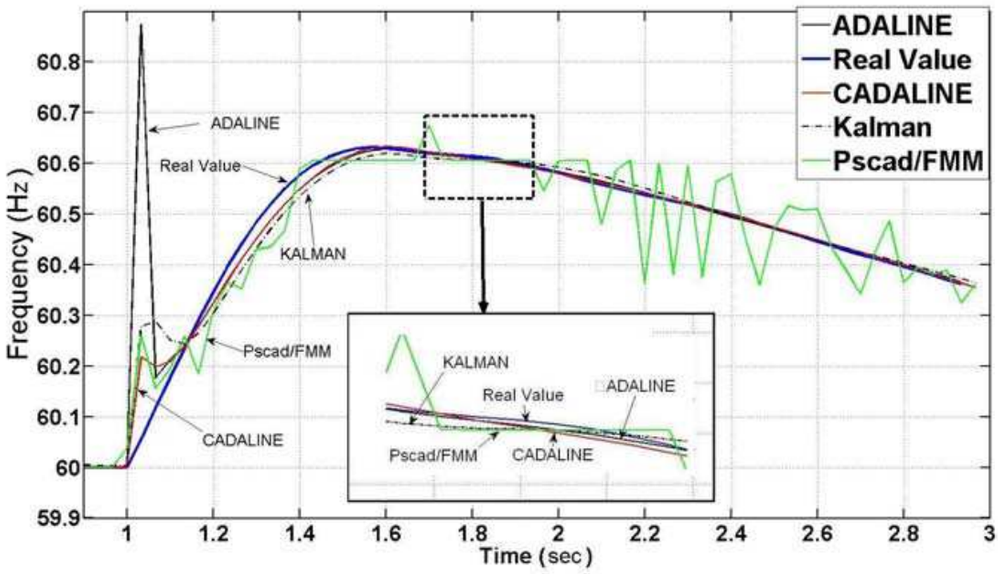

Fig. 10. Tracked frequency (Hz)

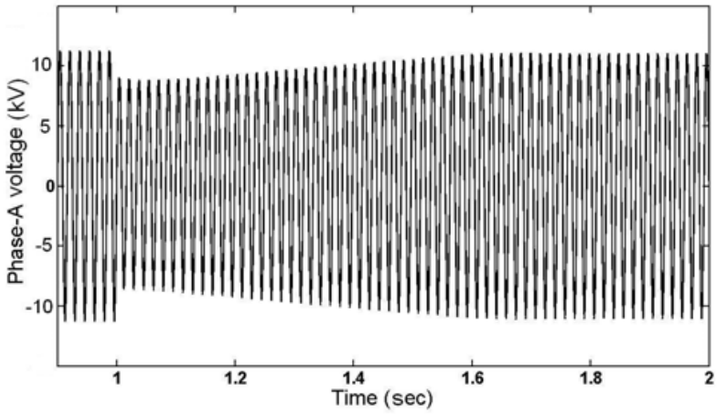

Fig. 11. Phase-A voltage (kV)

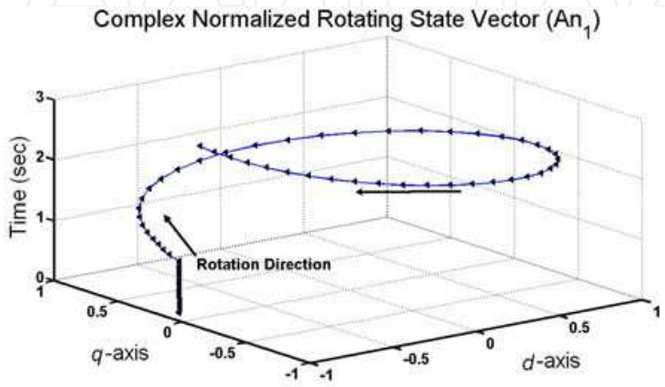

Fig. 12. Complex normalized rotating state vector (An_1)

6.3 Practical study

In this case, a practical example is represented. Voltage signal measurements are applied from the Marvdasht power station in Fars province, Iran. The recorder's sampling frequency (f_s) is 6.39 kHz and fundamental frequency of power system is 50 Hz. A fault between pahse-C and groung occurred on 4 March 2006. The fault location was 46.557 km from Arsanjan substation. Main information on the Marvdasht 230/66 kV station and other substation supplied by this station is given in Tables II and III, presented in Appendix II. Fig. 13 shows the performance of CADALINE, ADALINE, Kaman and DFT approaches. Besides, phase-C voltage and residual voltage are revealed in Fig. 14 (A) and Fig. 14 (B) respectively. Complex normalized rotating state vector (An_1) is shown in Fig. 15.

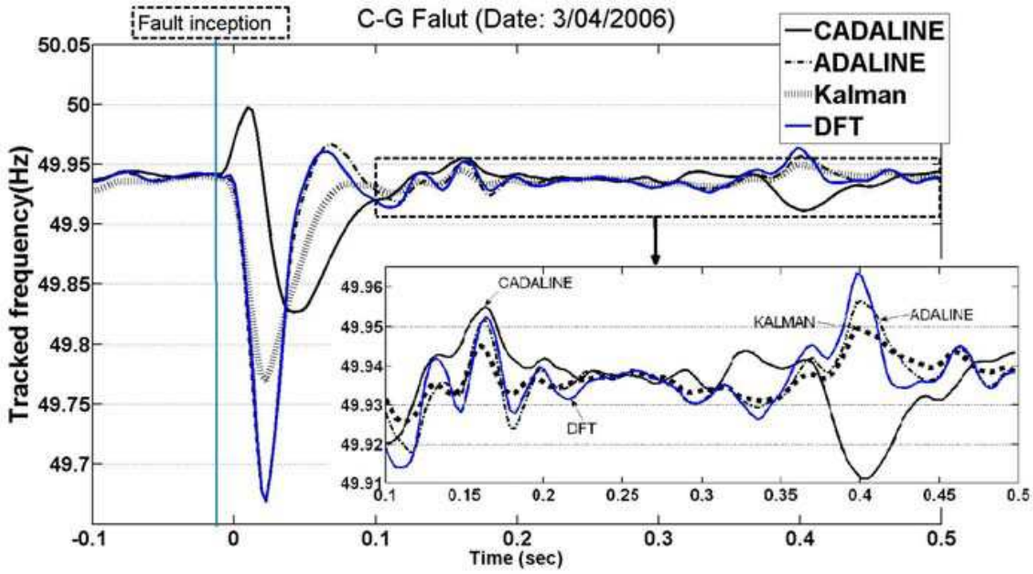

Fig. 13. Tracked frequency (Hz), case V.C.

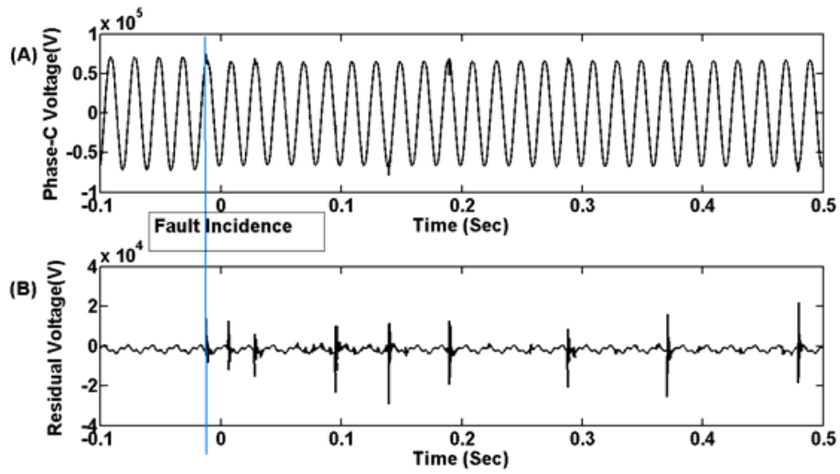

Fig. 14. (A): phase-C voltage and (B): residual voltage, case V.C.

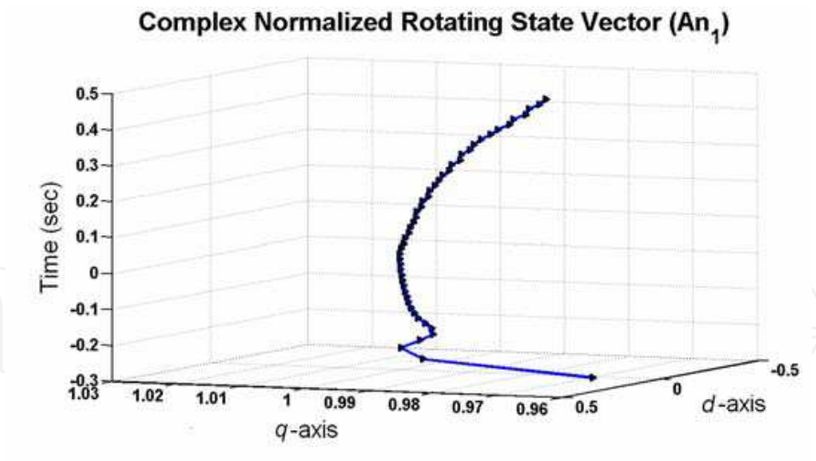

Fig. 15. Complex normalized rotating state vector (An_1), case V.C.

7. Conclusion

This section proposes an adaptive approach for frequency estimation in electrical power systems by introducing a novel complex ADALINE (CADALINE) structure. The proposed technique is based on tracking and analyzing a complex rotation state vector in *d*-*q* frame that appears when a frequency drift occurs. This method improves the convergence speed both in steady states and dynamic disturbances which include changes in base frequency of power system. Furthermore, the proposed method reduces the size of the state observer vector that has been used by simple ADALINE structure in other references. The numerical and simulation examples have verified that the proposed technique is far more robust and accurate in estimating the instantaneous frequency under various conditions compared with methods that have been reviewed in this section.

8. Appendices

8.1 Appendix I. multi-machine system information simulated in PSCAD/EMTDC software

1. Basic data of all generators are:
   Number of machines: 3
   Rated line-to-neutral voltage (RMS): 7.967 [kV]
   Rated line current (RMS): 5.02 [kA]
   Base angular frequency: 376.991118 [rad/sec]
   Inertia constant: 3.117 [s]
   Mechanical friction and windage: 0.04 [p.u.]
   Neutral series resistance: 1.0E5 [p.u.]
   Neutral series reactance: 0 [p.u.]
   Iron loss resistance: 300.0 [p.u.]
2. Fault characteristics:
   Fault inductance: 0.00014 [H]
   Fault resistance: 0.0001 [Ω]
3. Load characteristics:

Load active power: 190 [MW]
Load nominal line-to-line voltage: 13.8 [kV]

8.2 Appendix. II

Main information on the Marvdasht 230/66 (kV) station and other substation supplied by this station is given in Tables II and III.

NO.	SUBSTATION NAME	FEEDER NO. TAG	3-PHASE SHORT CIRCUIT CAPACITY (MVA)	1-PHASE SHORT CIRCUIT CAPACITY (MVA)
1	Marvdasht 230/66 (kV)	-	1460	1184
2	Marvdasht City	602	896	640
3	Mojtama	601	631	423
4	Kenare	607	1005	718
5	Sahl Abad	603	751	500
6	Dinarloo	604	203	121
7	Seydan	608	381	237
8	Arsanjan	605	145	84

Table II Marvdasht substation capacities

NO.	SUBSTATION NAME	FEEDER NO. TAG	3-PHASE SHORT CIRCUIT CURRENT (kA)	1-PHASE SHORT CIRCUIT CURRENT (kA)	$\lvert Z \rvert$ (Ω)
1	Marvdasht 230/66 (kV)	-	12.77169	10.35731	2.983562
2	Marvdasht City	602	7.837967	5.598548	4.861607
3	Mojtama	601	5.519818	3.70029	6.903328
4	Kenare	607	8.79147	6.280871	4.334328
5	Sahl Abad	603	6.569546	4.373866	5.800266
6	Dinarloo	604	1.775789	1.058475	21.45813
7	Seydan	608	3.332886	2.073212	11.43307
8	Arsanjan	605	1.268421	0.734809	30.04138

Table III Marvdasht substation three-phase and single-phase short circuit capacities and impedances ($\lvert Z \rvert$)

9. References

J.K. Wu, Frequency tracking techniques of power systems including higher order harmonics devices, Proceedings of the Fifth IEEE International Caracas Conference, vol. 1, (3–5 Nov. 2004), pp. 298–303.

M. Akke, Frequency estimation by demodulation of two complex signals, IEEE Trans. Power Del., vol. 12, no. 1, (Jan. 1997), pp. 157–163.

P.J. Moore, R.D. Carranza and A.T. Johns, Model system tests on a new numeric method of power system frequency measurement, IEEE Trans. Power Del., vol. 11, no. 2, (Apr. 1996), pp. 696–701.

M.M. Begovic, P.M. Djuric, S. Dunlap and A.G. Phadke, Frequency tracking in power networks in the presence of harmonics, IEEE Trans. Power Del., vol. 8, no. 2, (April 1993), pp. 480–486.

C.T. Nguyen and K.A. Srinivasan, A new technique for rapid tracking of frequency deviations based on level crossings, IEEE Trans. Power App. Syst., vol. 103, no. 8, (April 1984), pp. 2230–2236.

I. Kamwa and R. Grondin, Fast adaptive schemes for tracking voltage phasor and local frequency in power transmission and distribution systems, IEEE Trans. Power Del., vol. 7, no. 2, (April 1992), pp.789–795.

M.S. Sachdev and M.M. Giray, A least error square technique for determining power system frequency, IEEE Trans. Power App. Syst., vol. 104, no. 2, (Feb. 1985), pp. 437–443.

M.M. Giray and M.S. Sachdev, Off-nominal frequency measurements in electric power systems, IEEE Trans. Power Del., vol. 4, no. 3, (July 1989), pp. 1573–1578.

V.V. Terzija, M.B. Djuric and B.D. Kovacevic, Voltage phasor and local system frequency estimation using Newton-type algorithm, IEEE Trans. Power Del., vol. 9, no. 3, (Jul. 1994), pp. 1368–1374.

M.S. Sachdev, H. C. Wood and N. G. Johnson, Kalman filtering applied to power system measurements for relaying, IEEE Trans. Power App. Syst., vol. 104, no. 12, (Dec. 1985), pp. 3565–3573.

A.A. Girgis and T.L.D. Hwang, Optimal estimation of voltage phasors and frequency deviation using linear and nonlinear Kalman filter: Theory and limitations, IEEE Tran. Power App. Syst., vol. 103, no. 10, (1984), pp. 2943–2949.

A.A. Girgis and W.L. Peterson, Adaptive estimation of power system frequency deviation and its rate of change for calculating sudden power system overloads, IEEE Trans. Power Del., vol. 5, no. 2, (Apr. 1990), pp. 585–594.

T. Lobos and J. Rezmer, Real time determination of power system frequency, IEEE Trans. Instrum. Meas., vol. 46, no. 4, (Aug. 1997), pp. 877–881.

A.G. Phadke, J.S. Thorp and M.G. Adamiak, A new measurement technique for tracking voltage phasors, local system frequency, and rate of change of frequency, IEEE Trans. Power App. and Systems, vol. 102, no. 5, (May 1983), pp. 1025–1038.

J.Z. Yang and C.W. Liu, A precise calculation of power system frequency, IEEE Trans. Power Del., vol. 16, no. 3, (July 2001), pp. 361–366.

J.Z. Yang and C.W. Liu, A precise calculation of power system frequency and phasor, IEEE Trans. Power Del., vol. 15, no. 2, (Apr. 2000), pp. 494–499.

S.L. Lu, C.E. Lin and C.L. Huang, Power frequency harmonic measurement using integer periodic extension method, Elect. Power Syst. Res., vol. 44, no. 2, (1998), pp. 107–115.

P.J. Moore, R.D. Carranza and A.T. Johns, A new numeric technique for high speed evaluation of power system frequency, IEE Gen. Trans. Dist. Proc., vol. 141, no. 5 (Sept. 1994), pp. 529–536.

J. Szafran and W. Rebizant, Power system frequency estimation, IEE Gen. Trans. Dist. Proc., vol. 145, no. 5, (Sep. 1998), pp. 578–582.

A.A. Girgis and F.M. Ham, A new FFT-based digital frequency relay for load shedding, IEEE Trans. Power App. Syst., vol. 101, no. 2, (Feb. 1982), pp. 433–439.

H.C. Lin and C. S. Lee, Enhanced FFT-based parameter algorithm for simultaneous multiple harmonics analysis, IEE Gen. Trans. Dist. Proc., vol. 148, no. 3, (May 2001), pp. 209–214.

W.T. Kuang and A.S. Morris, Using short-time Fourier transform and wavelet packet filter banks for improved frequency measurement in a Doppler robot tracking system, IEEE Trans. Instrum. Meas., vol. 51, no. 3, (June 2002), pp. 440–444.

V.L. Pham and K. P. Wong, Wavelet-transform-based algorithm for harmonic analysis of power system waveforms, IEE Gen. Trans. Dist. Proc., vol. 146, no. 3, (May 1999), pp. 249–254.

V.L. Pham and K.P. Wong, Antidistortion method for wavelet transform filter banks and nonstationary power system waveform harmonic analysis, IEE Gen. Trans. Dist. Proc., vol. 148, no. 2, (March 2001), pp. 117–122.

M. Wang and Y. Sun, A practical, precise method for frequency tracking and phasor estimation, IEEE Trans. Power Del., vol. 19, no. 4, (Oct. 2004), pp. 1547–1552.

D.W.P. Thomas and M.S. Woolfson, Evaluation of a novel frequency tracking method, Transmission and Distribution Conference, vol. 1, (11–16 April 1999), pp. 248–253.

M.I. Marei, E.F. El-Saadany and M.M.A. Salama, A processing unit for symmetrical components and harmonics estimation based on a new adaptive linear combiner structure, IEEE Trans. Power Del., vol. 19, no. 3, (July 2004), pp. 1245–1252.

P.J. Moore, J.H. Allmeling and A.T. Johns, Frequency relaying based on instantaneous frequency measurement, IEEE Trans. Power Del., vol. 11, no. 4, (Oct. 1996), pp. 1737–1742.

D.W.P. Thomas and M.S. Woolfson, Evaluation of frequency tracking methods, IEEE Trans. Power Del., vol. 16, no. 3, (July 2001), pp. 367–371.

G. J. Retter, Matrix and Space-Phasor Theory of Electrical Machines, Akademiai Kiado, Budapest, Rumania, (1987).

G.H. Hostetter, Recursive discrete Fourier transformation, IEEE Trans. Speech Audio Process., vol. 28, no, 2, (1980), pp. 184–190.

R.R. Bitmead, A.C. Tsoi and P.J. Parker, A Kalman filtering approach to short-time Fourier analysis, IEEE Trans. Speech Audio Process., vol. 34, no. 6, (1986), pp. 1493–1501

T. Kailath, Linear Systems, Prentice-Hall, New Jersey, (1980).

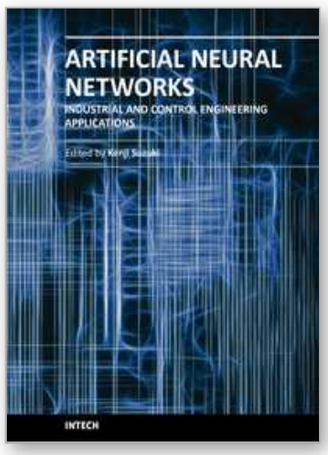

Artificial Neural Networks - Industrial and Control Engineering Applications

Edited by Prof. Kenji Suzuki

ISBN 978-953-307-220-3
Hard cover, 478 pages
Publisher InTech
Published online 04, April, 2011
Published in print edition April, 2011

Artificial neural networks may probably be the single most successful technology in the last two decades which has been widely used in a large variety of applications. The purpose of this book is to provide recent advances of artificial neural networks in industrial and control engineering applications. The book begins with a review of applications of artificial neural networks in textile industries. Particular applications in textile industries follow. Parts continue with applications in materials science and industry such as material identification, and estimation of material property and state, food industry such as meat, electric and power industry such as batteries and power systems, mechanical engineering such as engines and machines, and control and robotic engineering such as system control and identification, fault diagnosis systems, and robot manipulation. Thus, this book will be a fundamental source of recent advances and applications of artificial neural networks in industrial and control engineering areas. The target audience includes professors and students in engineering schools, and researchers and engineers in industries.

InTech Europe
University Campus STeP Ri
Slavka Krautzeka 83/A
51000 Rijeka, Croatia
Phone: +385 (51) 770 447
Fax: +385 (51) 686 166
www.intechopen.com

InTech China
Unit 405, Office Block, Hotel Equatorial Shanghai
No.65, Yan An Road (West), Shanghai, 200040, China
中国上海市延安西路65号上海国际贵都大饭店办公楼405单元
Phone: +86-21-62489820
Fax: +86-21-62489821

IntechOpen